Journal of Thermal Analysis and Calorimetry (2019) 138:4331–4340
https://doi.org/10.1007/s10973-019-08142-7

Synthesis, characterization and hydration analysis of Ba^{2+}-, Cu^{2+}- or Bi^{3+}-doped $CaO–Al_2O_3–ZrO_2$-based cements

Dominika Madej[1] · **Renata Boris**[2]

Received: 5 October 2018 / Accepted: 16 February 2019 / Published online: 5 March 2019

Abstract
This paper deals with the design, synthesis, hydration mechanism and hydration products of novel Ba^{2+}-, Cu^{2+}- or Bi^{3+}-doped $CaO–Al_2O_3–ZrO_2$-based cementitious materials used for heavyweight concrete mixes. The results of the heating microscopy thermal analysis indicated that both Cu and Bi in a $Ca_7ZrAl_6O_{18}$-based cement clinker can effectively reduce the sintering temperature by 150–200 °C. Incorporation of barium for the synthesis of calcium zirconium aluminate-based hydraulic binder increased its thermal resistance since Ba^{2+}-doped $Ca_7ZrAl_6O_{18}$ along with accessory $(Ca,Ba)ZrO_3$ with a perovskite-type structure and $BaAl_2O_4$ phases having high melting points were formed. The presence of metal ions, i.e., Cu^{2+} or Bi^{3+}, created conditions which were favorable for the formation of hexagonal calcium aluminate hydrates rather than the cubic one, as confirmed by coupled DSC–TG/EGA–MS thermal analysis techniques and X-ray diffraction. For the Ba^{2+} doping ions, this effect was the least noticeable. The effect of metal ions including Ba^{2+}, Cu^{2+} and Bi^{3+} on microstructural features of cement pastes was investigated by SEM–EDS. These doping ions strongly affected the morphologies of Ca–Al hydrates.

Keywords Simultaneous DSC–TG/EGA–MS · Gamma shielding cement composites · Cement hydration · Microstructure

Introduction

Calcium aluminate cement (CAC) is a mixture of the clinker phases calcium monoaluminate ($CaO·Al_2O_3$, $CaAl_2O_4$ or CA), dodecacalcium hepta-aluminate ($12CaO·7Al_2O_3$, $Ca_{12}Al_{14}O_{33}$ or $C_{12}A_7$), calcium dialuminate ($CaO·2Al_2O_3$, $CaAl_4O_7$ or CA_2) and other minor constituents like alumina. Quantities of these minerals to be formed were dependent upon the chemical composition of raw materials and the consequent molar ratios of CaO to Al_2O_3 [1–3].

✉ Dominika Madej
dmadej@agh.edu.pl

[1] Department of Ceramics and Refractories, Faculty of Materials Science and Ceramics, AGH University of Science and Technology, al. A. Mickiewicza 30, 30-059 Kraków, Poland

[2] Laboratory of Composite Materials, Institute of Building Materials, Vilnius Gediminas Technical University, Linkmenu Str 28, 08217 Vilnius, Lithuania

The hypothesis that the presence of foreign ions in the composition of given calcium aluminates may noticeably affect the sintering behavior and hydraulic properties of the mineral compounds of cement clinker can be formulated. Hence, investigations of the extent of solid solution occurring in calcium aluminates are important to cement technologists. The dopant ions replace cations in the crystalline lattice of cementitious compounds leading to the formation of a substitutional solid solution. Such a replacement may cause distinct deformations and distortions of the crystalline lattice. Hence, the crystal-chemical environment for Ca and Al atoms changes, as well as the electron-binding energies [4]. Going into details, the modification of hydraulic properties of the cementitious minerals may be achieved by the incorporation of foreign ions, including cations and anions, into both sublattices. Many examples can be quoted among the clinker minerals, some of which were the object of more or less recent studies by several cement chemistry experts. Among the many possible examples, we can quote here tricalcium aluminate ($3CaO·Al_2O_3$, $Ca_3Al_2O_6$ or C_3A), dodecacalcium hepta-aluminate and calcium monoaluminate. A general formula of C_3A can be modified by cations like Na^+, K^+, Mg^{2+}, Fe^{3+}, Si^{4+} and others [5–8]. As a result of experimental research, it was found that these foreign ions alter the crystal structure and the hydraulic activity of OPC (ordinary Portland cement) clinker phase C_3A. As an another example, the substitution of Ca^{2+} by Sr^{2+} in this phase can induce some modifications in the structure to obtain the mixed Ca/Sr aluminates $Ca_{3-x}Sr_xAl_2O_6$, $3 \leq x \leq 0$, reactions and properties [9]. Further, the features of the X-ray diffraction pattern suggest that the incorporation of Sn ions within C_3A lattice caused the deformation of lattice parameters since diffraction peak positions show a light shifting [10]. Besides, studies of the effect of Na^+ doping of CA, $C_{12}A_7$ and C_3A have identified a C_3A–Na_2O solid solution of different symmetry form, which was found to decompose into $NaAlO_2$ and CaO upon doping with larger amounts of Na_2O doping additives [11]. Tian et al. [12] synthesized clinker that has Na_2O-containing minerals ($2Na_2O{\cdot}3CaO{\cdot}5Al_2O_3$ and $Na_2O{\cdot}Al_2O_3$) and Na_2O-doped $C_{12}A_7$ with a poor crystalline structure. From the structural point of view, Sr^{2+} and Ba^{2+} ions are widely used to replace Ca^{2+} ions in the crystal structure of calcium aluminates to form the series of both $CaAl_2O_4$-$SrAl_2O_4$ and $BaAl_2O_4$-$CaAl_2O_4$ solid solutions [13–16]. The review of the literature points to the possibility of modification of hydraulic properties through structural modifications by doping with different cations. In recent years, $Ca_7ZrAl_6O_{18}$ and Sr^{2+}-doped $Ca_7ZrAl_6O_{18}$ phases arouse interest mainly due to their unique hydraulic properties to produce a rapid curing mortar [17–19].

Following the review of literature, three main research objectives for this paper were undertaken. Firstly, sintering additives are able to activate changes in the sintering temperature and kinetics of the clinker phases. Secondly, hydration kinetics of clinker phases can be affected by the presence of foreign cations. Thirdly, hydration products may sorb foreign ions by surface processes, or they may incorporate the ions in their structure by a solid solution process. Despite the importance of calcium aluminates and calcium zirconium aluminate and the potential incorporation of foreign cations such as Ba^{2+}, Cu^{2+} and Bi^{3+}, there is a lack of research on the effect of ions doping on the clinker formation in the CaO–Al_2O_3–ZrO_2 system. Hence, this study will fill the gap in the literature concerning synthesis, formation mechanism and hydraulic activity of the metals (Me^{2+},Me^{3+})-doped CaO–Al_2O_3–ZrO_2 cementitious materials.

Experimental

Synthesis and methods of investigation

The present study deals with incorporating the BaO, CuO or Bi_2O_3 oxides in the raw metal for the synthesis of $Ca_7ZrAl_6O_{18}$-based cement clinkers. The raw metal for the synthesis of Ba^{2+}-, Cu^{2+}- or Bi^{3+}-doped calcium zirconium aluminate was prepared by mixing of calcium carbonate ($CaCO_3$), aluminum oxide (Al_2O_3), zirconia (ZrO_2) and $BaCO_3$, CuO or Bi_2O_3 in the mass ratios required for compositions of $6.5CaO{\cdot}0.5BaO{\cdot}ZrO_2{\cdot}3Al_2O_3$, $6.5CaO{\cdot}0.5CuO{\cdot}ZrO_2{\cdot}3Al_2O_3$ and $7CaO{\cdot}ZrO_2{\cdot}0.5Bi_2O_3{\cdot}3Al_2O_3$, respectively. The reference pure clinker mineral $Ca_7ZrAl_6O_{18}$ was prepared by mixing reagent-grade products in the molar ratio of $7CaO{:}3Al_2O_3{:}ZrO_2$. The homogenization of all batches was performed in a laboratory ball mill for 2 h. Then, the homogenized powders were pressed under pressure of ca. 30 MPa to cylindrical samples of 2 cm in length and diameter. A two-step firing procedure was used to minimize any inhomogeneity of samples, as this has been known to occur with one-step firing processes. The first calcination step was performed at temperature of 1200 °C with a holding time of 10 h. The pellets calcined were ground, homogenized and uniaxially pressed again under 50 MPa. Variation of the second sintering temperature, i.e., 1450 °C (reference and Ba-doped samples) and below 1300 °C (Cu- and Bi-doped samples), depended on the modifying cations. The sintering time was 20 h.

The heating microscopy thermal analysis (HMTA) was applied to study the dimensional changes versus temperature during heat treatment process of the Ba^{2+}-, Cu^{2+}- or Bi^{3+}-doped C_7A_3Z. To this purpose, the powdered sample calcined at 1200 °C was used to prepare small cubes of 3 mm height, in a manual press. The changing of the samples shape was conducted by Carl Zeiss MH01 microscope at a heating rate of 10 °C min^{-1}. The data of the sample height were collected at intervals of 10 °C during the experiment, and shrinkage curves were obtained. The relative height change of the sample (δ_h) was calculated according to formula 1.

$$\delta_h(T) = \frac{h(T) - h_0}{h_0} \times 100/\% \quad (1)$$

where h_0, initial height of the sample; $h(T)$, height of the sample at elevated temperature T.

Microstructure of the ceramic sample was characterized by scanning electron microscopy (SEM) equipped with an energy-dispersive X-ray spectroscopy (EDS) system to allow for the chemical analysis. Sample surfaces were ground and polished with a 1 μm diamond suspension. Samples were then coated with a very thin layer of carbon and observed under NOVA NANO SEM 200 (from FEI EUROPE COMPANY) and analyzed with EDS instrument (from EDAX).

Cement paste preparation and methods of investigation

The other samples were powdered for the XRD measurement, and the dry cement powders were mixed with water (w/c ratio 1.0). The cement paste samples were conditioned at 50 °C and 85% relative humidity for 48 h. The microstructures of hardened cement pastes were derived largely from examination of fracture surfaces using SEM–EDS. Finally, the samples were washed two or three times more with 100% acetone to remove the remaining water. In studies of the thermal behavior and decomposition of the hydrated compounds formed in fully hydrated pastes, the typical thermal analysis techniques used in addition to thermogravimetry (TG) were differential scanning calorimetry (DSC) and evolved gas analysis (EGA). For this purpose, NETZSCH STA 449 F5 Jupiter coupled to QMS 403 D Aëolos was used. The following conditions were maintained during simultaneous DSC–TG–EGA run of the samples: heating rate—10 °C min^{-1}, atmosphere—air, sample mass—25 mg, reference material—alumina.

Proof of crystalline mineral phases in both unhydrated and hydrated cement pastes was performed by X-ray detection (XRD). The X-ray analysis was performed by a X'Pert Pro PANalytical X-ray diffractometer. The following conditions were maintained during XRD run of the samples: CuKα radiation, step size of 0.02° 2-theta, a scan range from 5.00° to 40°, temperature 25 °C.

Results and discussion

Heating microscopy of Ba^{2+}-, Cu^{2+}- or Bi^{3+}-doped C_7A_3Z

Calcined Ba^{2+}-, Cu^{2+}- or Bi^{3+}-doped C_7A_3Z samples sintering evaluation was done by heating microscopy thermal analysis (HMTA). The relative height changes of the sample (δ_h) versus temperature were presented as expansion and/or shrinking curves and are shown in Fig. 1. This figure shows, as examples, the heating microscope images registered at 1390 °C. Compared to the respective initial height of each sample, there was a mean shrinkage of ca. 21% (Cu-doped sample) and ca. 50% (Bi-doped sample) at 1390 °C, which was promoted by the presence of the liquid phase formed during the sintering process. The effect is clearly visible for Bi-doped sample. The lower sintering temperature of both samples as a dimensional variation corresponding to the − 2% with respect to the first image acquired, which is taken to be 100%, was established as ca. 1280 °C (Cu-doped sample) and ca. 1260 °C (Bi-doped sample). Hence, it was found that Cu and Bi in a $Ca_7ZrAl_6O_{18}$-based cement clinker can effectively reduce the sintering temperature by 150–200 °C, compared with both pure and Ba-doped $Ca_7ZrAl_6O_{18}$.

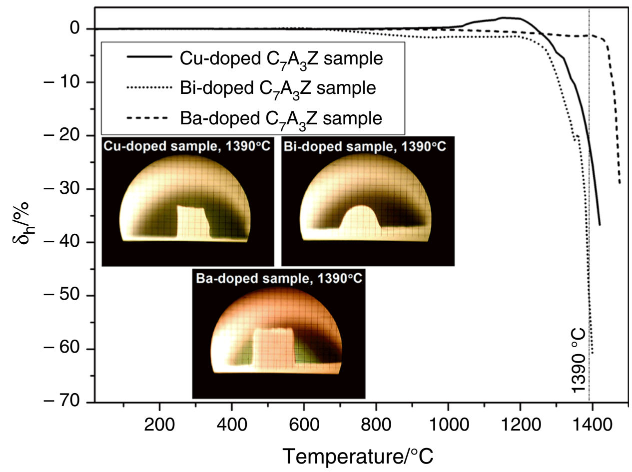

Fig. 1 Shrinkage curves of Cu-, Bi- and Ba-doped C_7A_3Z sample

Phase composition and microstructure of Ba^{2+}-, Cu^{2+}- or Bi^{3+}-doped C_7A_3Z

This section uses several analytical techniques (XRD and SEM–EDS) for the analysis of undoped C_7A_3Z and the Ba-, Cu- and Bi-doped C_7A_3Z samples, aiming to identify different phases within the sinters. The results of XRD analysis of the samples as-synthesized are presented in Fig. 2a–d. The diffraction peaks are well matched to the corresponding JCPDS card data, and results are summarized in Table 1. The results in Figs. 3–6 show the effect of ion doping on the microstructure of the C_7A_3Z-based sintered samples.

In the XRD pattern of the undoped C_7A_3Z sample (Fig. 2a), all the main peaks related to pure heptacalcium zirconium hexaaluminate (JCPDS No. 98-018-2622). Figure 2b-d shows the enlarged XRD patterns for the synthesized Cu-, Bi- and Ba-doped samples corresponding to (321), (231), (400), (222) and (040) planes, which indicate significant shifts of the diffraction peaks for all the metal-doped samples. The reason for the left shift (Fig. 2d) is due to the substitution of Ba^{2+} at the Ca^{2+} site of the lattice. Two cations Ca^{2+} and Ba^{2+} have difference in their ionic radii (1.14 Å and 1.49 Å), and hence, one should expect shift in X-ray diffraction peaks. Likewise, Fig. 2c shows a clear left shift of all 2-theta values. With all substituted samples besides the metal-doped calcium zirconium aluminate as major phase, the crystalline secondary phases appeared in all cases. Secondary phases were identified by

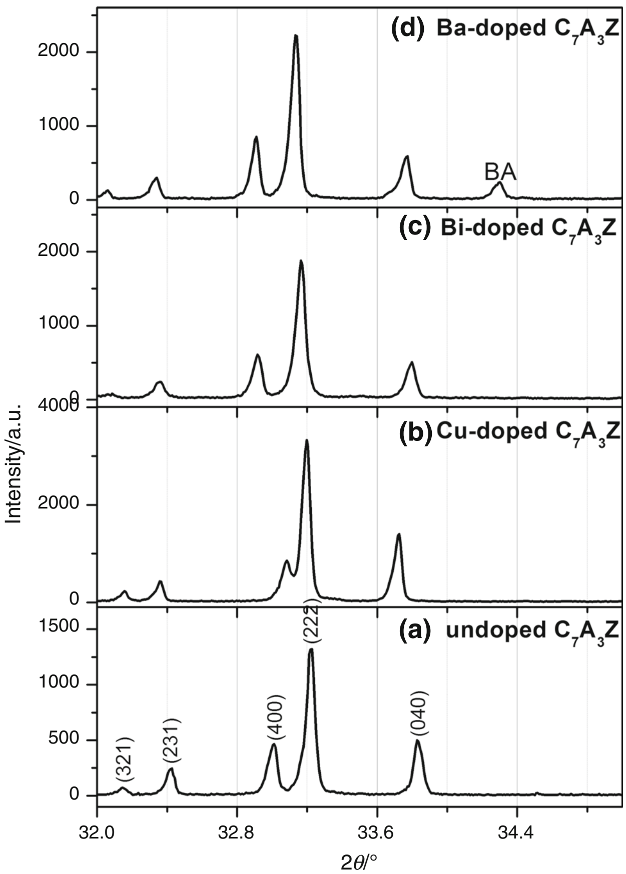

Fig. 2 X-ray diffraction patterns of calcium zirconium aluminate (a) and doped with copper oxide (b), bismuth oxide (c) and barium oxide (d). BA = $BaAl_2O_4$ as an accessory phase

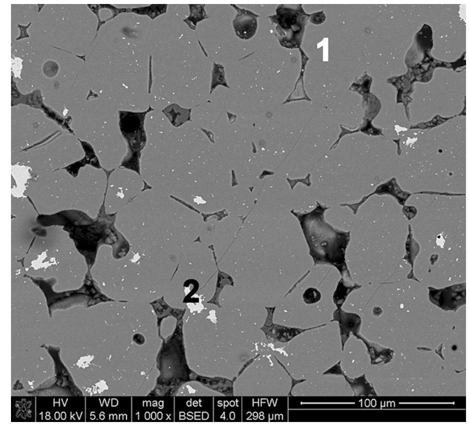

Fig. 3 SEM micrograph of undoped C_7A_3Z sample

JCPDS cards and are listed in Table 1. Although an interesting case can be seen with the sample sintered with copper oxide additive (Fig. 2b), some of the peak positions of the line profile shifted to a lower angle ((231), (222) and (040)), while the others shifted to higher angle (400). This non-uniform shift of peak positions in XRD pattern (Fig. 2b) can probably be caused by the "non-uniform" lattice distortion of $Ca_7ZrAl_6O_{18}$ compound. It is noteworthy, that, no diffraction peaks from and Cu-, Bi- and Ba-containing minor or accessory phases were detected in the range 2θ from 32° to 35° (Fig. 2a–d), indicating that these metal ions have partly incorporated into $Ca_7ZrAl_6O_{18}$ lattice.

SEM–EDS analysis was used to confirm the chemical compositions and appearance of different phases. Microstructure observations confirmed that different microstructures correspond well to the different doping ions. Figure 3 shows the typical microstructure of as-sintered coarse-grained calcium zirconium aluminate (point 1 in Fig. 3) with randomly dispersed inclusions of calcium zirconate (point 2 in Fig. 3).

The sintered Cu-doped C_7A_3Z sample exhibits mixed coarse-grained (point 1 in Fig. 4a) and fine-grained (point 2

Table 1 Crystalline phases in undoped, copper oxide-, bismuth oxide- and barium oxide-doped sintered samples identified by X-ray diffraction, according to JCPDS cards and confirmed by SEM–EDS

Sample	Phase	JCPDS Card No.
Undoped C_7A_3Z	$Ca_7ZrAl_6O_{18}$ +++	98-018-2622
	$CaZrO_3$ +	00-035-0790
Cu-doped C_7A_3Z	$Ca_7ZrAl_6O_{18}$ +++	98-018-2622
	Cu-containing phase +	Unmatched to JCPDS card data, but confirmed by SEM–EDS
	$CaZrO_3$ +	00-035-0790
Bi-doped C_7A_3Z	$Ca_7ZrAl_6O_{18}$ +++	98-018-2622
	$4.2CaO\cdot5.8Bi_2O_3$ ++	00-049-1542
	$CaZrO_3$ +	00-035-0790
Ba-doped C_7A_3Z	$Ca_7ZrAl_6O_{18}$ +++	98-018-2622
	$Ba_{0.8}Ca_{0.2}ZrO_3$ +	98-009-7471
	$BaAl_2O_4$ +	98-001-6845

+++ Major, ++ Minor, + Accessory

in Fig. 4a) microstructures. Figure 4b shows the elemental analyses of the main mineral of sintered matrix in the form of Cu-doped $Ca_7ZrAl_6O_{18}$. According to the SEM observations (Fig. 5a), the sintering products of Bi-doped C_7A_3Z sample are formed through a liquid phase. As shown in Fig. 5a, in the connection area, the minor phase is the calcium bismuth oxide melt, which is confirmed by EDS analysis (point 2). The main phase is in the form of Bi-doped $Ca_7ZrAl_6O_{18}$, which is confirmed by EDS analysis (Fig. 5b). Figure 6a is an example of a fine and homogenous microstructure of the Ba-doped $Ca_7ZrAl_6O_{18}$ (point 1) with secondary phases such as $BaAl_2O_4$ (point 2) and $(Ca,Ba)ZrO_3$ (point 3). The results discussed in this section points to the general conclusion that the doping of Ba^{2+}, Cu^{2+} and Bi^{3+} ions induces microstructural changes in C_7A_3Z samples.

Phase composition of Ba^{2+}-, Cu^{2+}- or Bi^{3+}-doped hydrated C_7A_3Z cements

X-ray diffraction patterns of all the samples were obtained at 48 h from mixing. A control paste was prepared from $Ca_7ZrAl_6O_{18}$ without any doping ions. The powder X-ray diffraction patterns of the undoped hydrated C_7A_3Z, Ba-

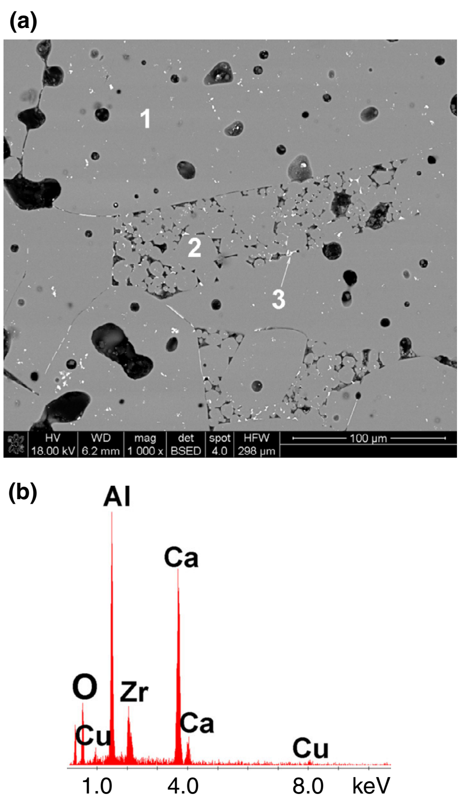

Fig. 4 **a** SEM micrograph of Cu-doped C_7A_3Z sample. EDS analysis in points 1 and 2—Cu-doped $Ca_7ZrAl_6O_{18}$, 3—Cu-containing accessory phase. **b** Typical SEM–EDS spectrum of Cu-doped $Ca_7ZrAl_6O_{18}$ in points 1 and 2 of Fig. 4a

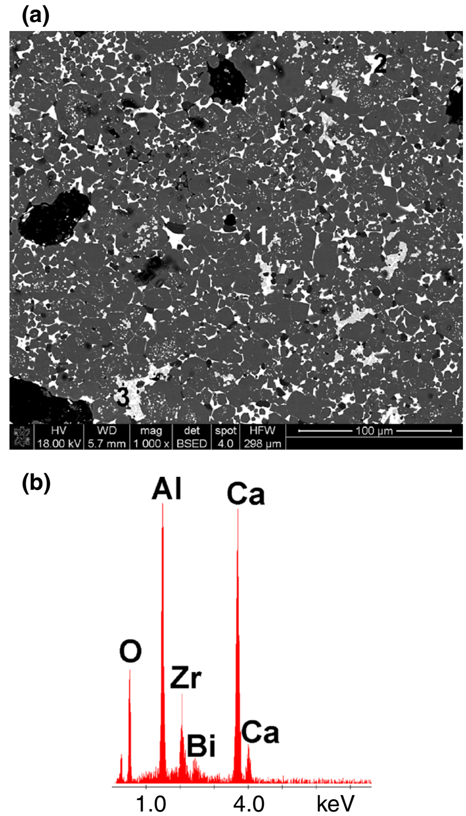

Fig. 5 **a** SEM micrograph of Bi-doped C_7A_3Z sample. EDS analysis in point 1 Bi-doped $Ca_7ZrAl_6O_{18}$, 2—calcium bismuth oxide minor phase, 3—$CaZrO_3$. **b** Typical SEM–EDS spectrum of Bi-doped $Ca_7ZrAl_6O_{18}$ in point 1 (**a**)

doped hydrated C_7A_3Z, Cu-doped hydrated C_7A_3Z and Bi-doped hydrated C_7A_3Z are illustrated in Fig. 7. Almost all the peaks of the XRD pattern in Fig. 7A-a can be indexed to the pure cubic phase $Ca_3Al_2O_6H_2O_6$ (JCPDS Card, No. 01-071-0735), meaning that the hydration of the $Ca_7ZrAl_6O_{18}$ phase is very fast and thus the consumption is noticeable during the 48 h. The results of the secondary phases detected by XRD agree with the phase equilibria of $CaO–Al_2O_3–H_2O$ system and the results presented elsewhere [20, 21] well.

The diffraction patterns of the Ba-, Cu- and Bi-doped hydrated C_7A_3Z sample reveal a multiphase character, with the stable cubic phase $Ca_3Al_2O_6H_2O_6$ as the main hydration product and hexagonal hydrates being the main secondary phases. It needs to be highlighted that two thermodynamically unstable calcium aluminate hydrate phases C_2AH_8 and C_4AH_{19} were formed in the metal ion-doped C_7A_3Z samples (Fig. 7A b–d). X-ray patterns of these two phases are almost coincident, so it was difficult to distinguish these two phases. Usually, the XRD of the C_2AH_8 shows the 100% intensity peak centered typically at $2\theta = 8.170°$ ($d = 10.81270$ Å), whereas a characteristic peak of the C_4AH_{19} is centered at $2\theta = 8.301°$

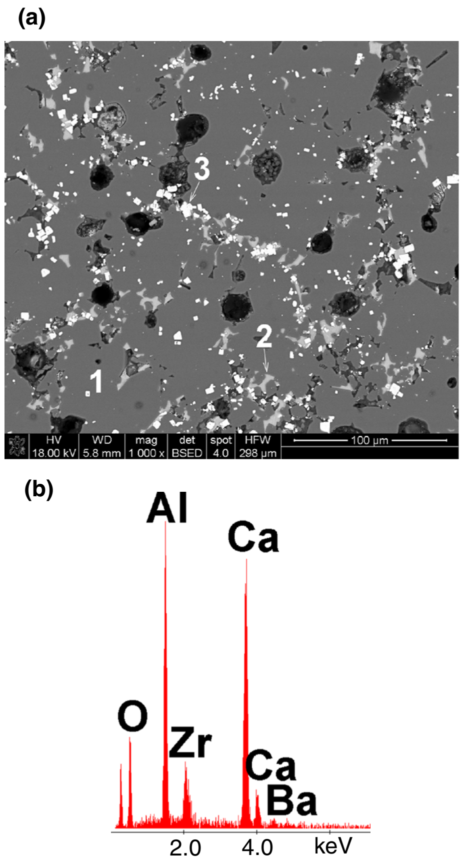

Fig. 6 **a** SEM micrograph of Ba-doped C_7A_3Z sample. EDS analysis in point 1 Ba-doped $Ca_7ZrAl_6O_{18}$, 2—$BaAl_2O_4$, 3—(Ca,Ba)ZrO_3. **b** Typical SEM–EDS spectrum of Ba-doped $Ca_7ZrAl_6O_{18}$ in point 1 (**a**)

(d = 10.64350 Å). In the metal ion-doped C_7A_3Z samples, the peak that corresponds to hexagonal hydrates shifts toward the higher 2θ angles, as can be observed in Fig. 7B. It is also note worthy that in diffraction patterns of pastes containing Cu and Bi, the peaks of both C_2AH_8 and C_4AH_{19} have higher intensity than the one in sample containing Ba. A general conclusion that one can draw from the research reviewed in this part is that doping of $Ca_7ZrAl_6O_{18}$ phase especially with Cu and Bi and also Ba promotes the formation of metastable hexagonal phases. Further, C_2AH_8 hydrate is more produced in hardened Cu-doped C_7A_3Z cement paste than in other hardened cement pastes. These results also confirmed the expected deceleration of $Ca_7ZrAl_6O_{18}$ cement hydration due to the effect of "foreign metal" doping. The unhydrated residuals were recognized in XRD patterns by the presence of the most intense peaks of $Ca_7ZrAl_6O_{18}$ (Fig. 7B b–d).

Dehydration mechanism of Ba^{2+}-, Cu^{2+}- or Bi^{3+}-doped hydrated C_7A_3Z determined by combined DSC–TG–EGA–MS

Combined with the X-ray diffraction analysis, DSC–TG–EGA–MS curves of undoped C_7A_3Z and the Ba-, Cu- and Bi-doped C_7A_3Z samples can be a further qualitative analysis of the changes in the composition of the hydration products due to the effect of "foreign metal" doping. TG, DSC and EGA–MS curves are shown in Fig. 8a–d. Typically, the DSC curves are used merely as fingerprints for the identification of different crystalline and non-crystalline hydrates which are obtained via hydration of calcium aluminate (CACs) and $Ca_7ZrAl_6O_{18}$ cements under different curing conditions [22]. For example, Ukrainczyk et al. [23] studied dehydration of a layered double hydroxide C_2AH_8. From DTG curve, they concluded that the thermal decomposition of C_2AH_8 is an endothermic process which takes place in three main steps, at about 110, 175 and 300 °C (or at 100, 160–200 and 250–300 °C [24]). Fleisher [25] and Hill [26] have reported that the thermal decomposition temperature of C_4AH_{13-19} is in the range of 200–280 °C or at 250 °C. Monocarboaluminate $3CaO{\cdot}Al_2O_3{\cdot}CaCO_3{\cdot}11H_2O$ ($C_4A\bar{C}H_{11}$; $\bar{C}$=CO_2) gives a typical broad endothermic peak in the temperature range of 160–200 °C, located similar to C_2AH_8 [27]. According to the result given by Barbakadze et al. [24], the cubic compound C_3AH_6 displays an endothermic effect at 330 and 500–520 °C. Other references to thermal stability of hydrated calcium aluminates can be found in Ref. [28] and presented as follows: The endothermic effects in the range 140–150 °C and 240–285 °C are attributed to hexagonal C_2AH_8 and C_4AH_{13} hydrates, respectively, and the two endothermic effects at 290–300 °C and 460–500 °C are attributed to the cubic C_3AH_6 hydrates.

Typical DSC plot of undoped hardened C_7A_3Z paste cured for 48 h at the curing temperature of 50 °C is shown in Fig. 8a in which the endothermic peaks at 264 and 302 °C corresponding to H_2O^+ emission are attributed to $Al(OH)_3$ and C_3AH_6, respectively [21]. Differential thermal analysis of the Cu-doped hydrated C_7A_3Z sample helped to establish that among the calcium aluminate hydrates, the most possible is C_2AH_8, which displayed an endothermic effect at 88, 145 and 292 °C (Fig. 8b), while the last endothermic effect at 292 °C also represents the dehydration of C_3AH_6. Cement pastes containing foreign Ba or Bi ions display similar evolved gas profiles for H_2O^+ (Fig. 8c–d) with the dominant peak present around 290 °C, which could be due to dehydration of crystalline C_3AH_6. Other endothermic effects corresponding to H_2O^+ emission at 77 and 139 °C in Fig. 8c and at 124 and 146 °C in Fig. 8d due to C_2AH_8 are also observed. The endothermic

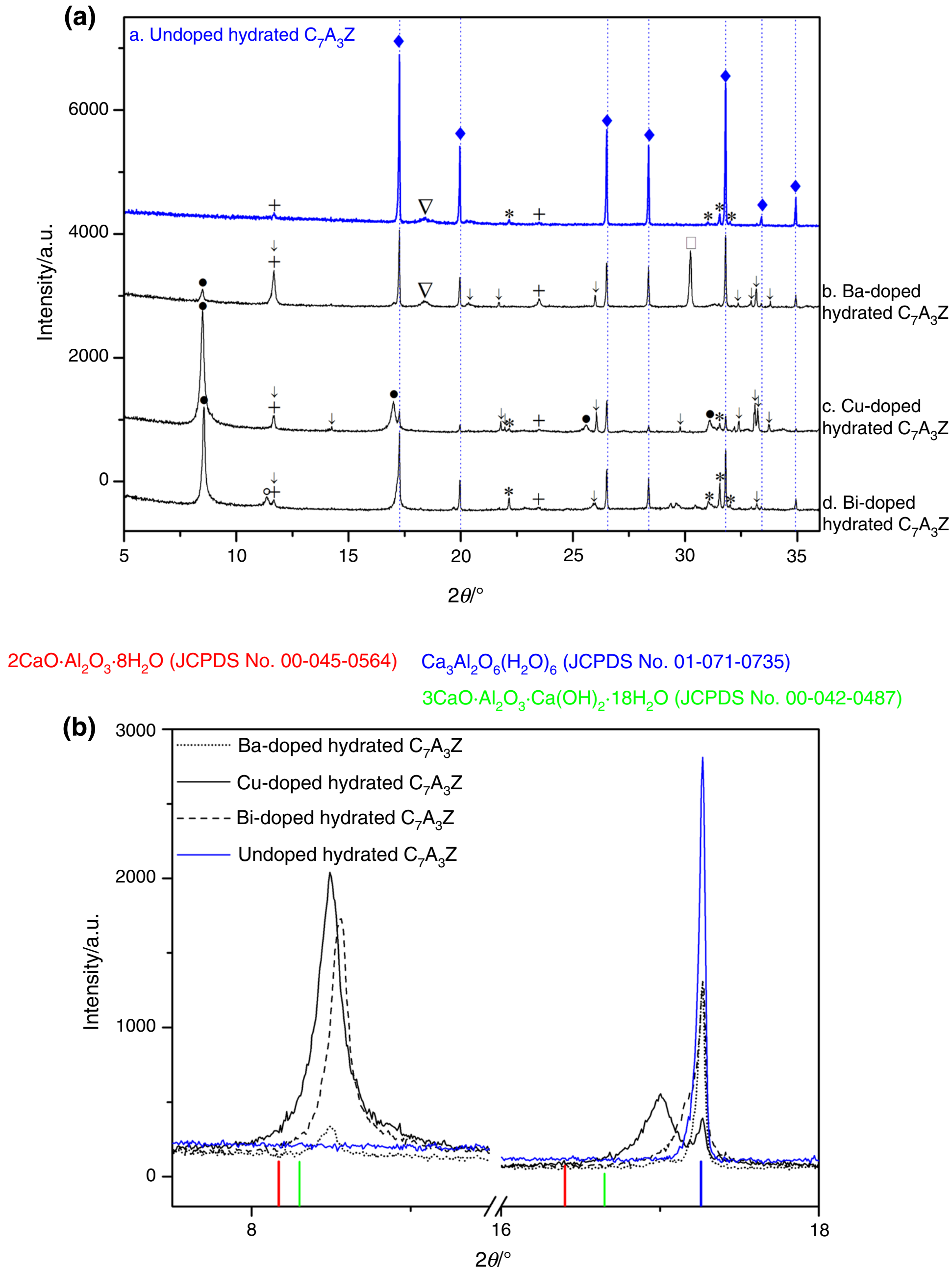

Fig. 7 **A** X-ray diffraction patterns of the undoped hydrated C_7A_3Z (a), Ba-doped hydrated C_7A_3Z (b), Cu-doped hydrated C_7A_3Z (c), Bi-doped hydrated C_7A_3Z (d), where filled diamond $Ca_3Al_2O_6H_2O_6$ (JCPDS No. 01-071-0735), filled circle $3CaO·Al_2O_3·Ca(OH)_2·18H_2O$ (JCPDS No. 00-042-0487) and $2CaO·Al_2O_3·8H_2O$ (JCPDS No. 00-045-0564), ∇ $Al(OH)_3$ (JCPDS No. 00-007-0324), +$3CaO·Al_2O_3·CaCO_3·11H_2O$ (JCPDS No. 00-041-0219), open square: $Ba_{0.8}Ca_{0.2}ZrO_3$ (JCPDS No. 98-009-7470), open circle $Ca_2Al(OH)_7·3H_2O$ (JCPDS No. 00-016-0333), ↓ $Ca_7ZrAl_6O_{18}$ (JCPDS No. 98-018-2622), * $CaZrO_3$ (JCPDS No. 00-035-0790) and **B** over a narrow range of 2 theta

effect caused by dehydration of $3CaO·Al_2O_3·Ca(OH)_2·18H_2O$, which was identified previously by XRD in the Ba-, Cu- and Bi-doped C_7A_3Z samples, overlaps with the broad endothermic effect at ca. 290 °C which is due to ongoing decomposition of C_3AH_6. Also, the endothermic peaks of $C_4A\bar{C}H_{11}$ and $Ca_2Al(OH)_7·3H_2O$ phases were not readily discernible on the curves, indicating thereby that the amount of both $C_4A\bar{C}H_{11}$ (Fig. 8a–d) and $Ca_2Al(OH)_7·3H_2O$ (Fig. 8c) formed was very small. There were observed only traces of $C_4A\bar{C}H_{11}$ (Fig. 7A a–d) and $Ca_2Al(OH)_7·3H_2O$ (Fig. 7A d) in the XRD patterns.

The results discussed in this section led us to the general conclusion that the ability of cement pastes to develop stable cubic hydrate C_3AH_6 and AH_3 (gibbsite) can be ranked as follows, according to both the presence of unhydrated residues and the formation of metastable and stable phases: undoped hydrated C_7A_3Z > Ba-doped hydrated C_7A_3Z > Bi-doped hydrated C_7A_3Z > Cu-doped hydrated C_7A_3Z.

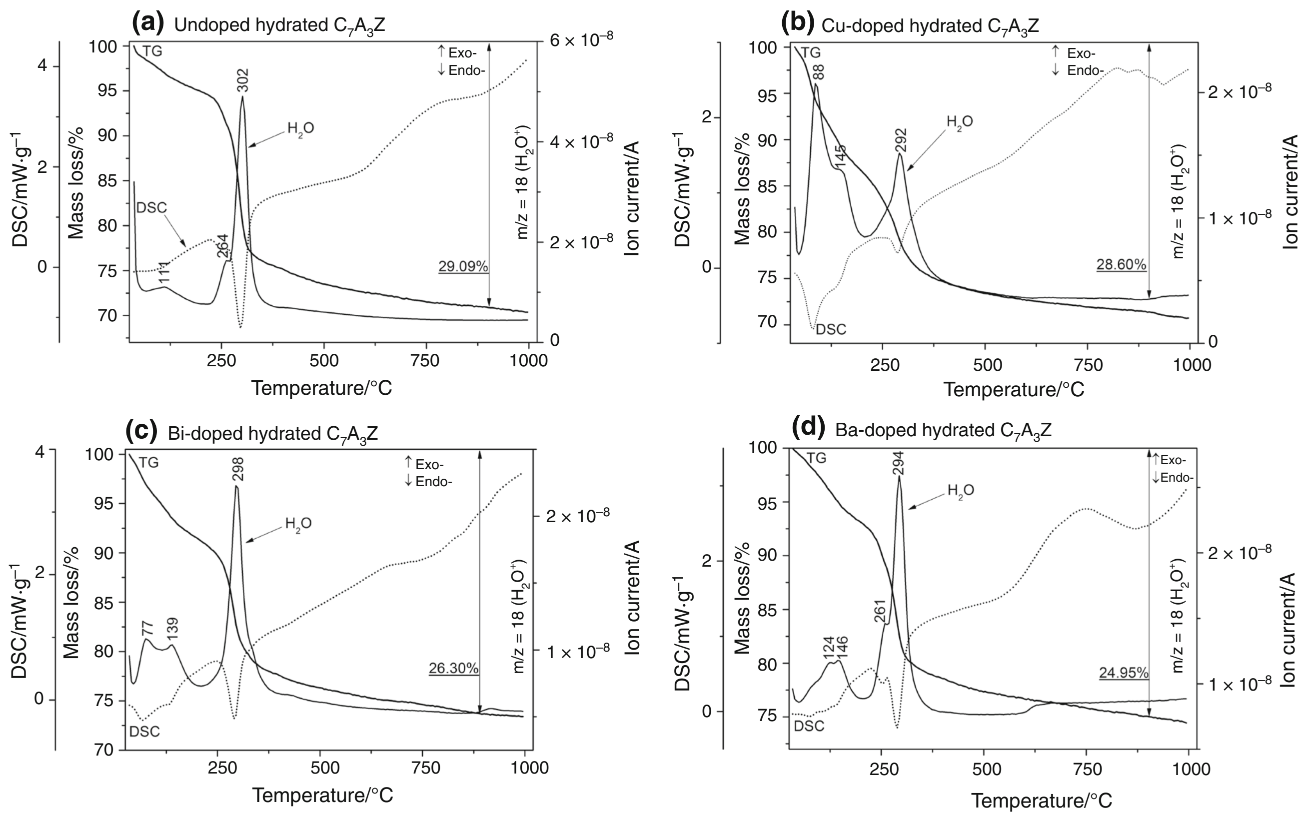

Fig. 8 Simultaneous DSC–TG curves of the undoped hydrated C_7A_3Z (**a**), Cu-doped hydrated C_7A_3Z (**b**), Bi-doped hydrated C_7A_3Z (**c**) and Ba-doped hydrated C_7A_3Z (**d**) measured in air at flow rate 50 mL min^{-1} (heating rate 10 °C min^{-1}, initial mass of sample 25 mg). EGA–gas evolution curve for representative mass spectroscopic ion fragments of H_2O^+ (m/z = 18) vapors

Microstructure of Ba^{2+}-, Cu^{2+}- and Bi^{3+}-doped hydrated C_7A_3Z

In this experiment, the morphology of hydrates between hardened undoped C_7A_3Z cement paste and doped with three different metal ions (Ba^{2+}, Cu^{2+} and Bi^{3+}) was further observed with SEM, so as to provide a clearer analysis. A typical SEM micrograph of the undoped $Ca_7ZrAl_6O_{18}$ hydrated at 50 °C for 48 h is presented in Fig. 9, showing the somewhat spherical, cubic C_3AH_6 crystals and agglomerated rounded gibbsite crystals. Figure 10 shows an SEM image of closely packed thin plates of hexagonal calcium aluminate hydrate with composition C_2AH_8 (point 1) formed within the Cu-doped C_7A_3Z cement paste. Crystalline hydrates, such as C_3AH_6 (point

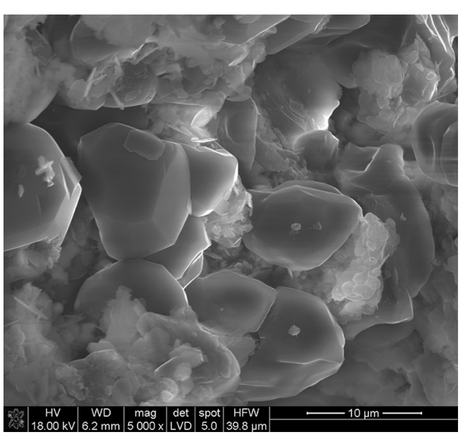

Fig. 9 SEM image of hardened undoped C_7A_3Z cement paste cured at 50 °C for 48 h

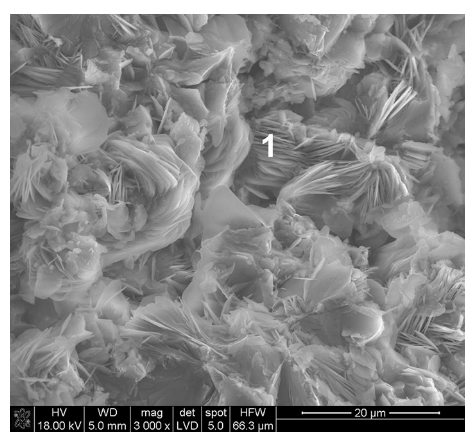

Fig. 10 SEM image of hardened Cu-doped C_7A_3Z cement paste cured at 50 °C for 48 h. EDS analysis in point 1—hexagonal crystals of calcium aluminate hydrates

1) in the form of cubic crystals and C_2AH_8 (point 2) as a thin well-formed hexagonal platelet crystals, were clearly distinguished in the SEM image of hardened Bi-doped C_7A_3Z cement paste (Fig. 11). This microstructure also consists of thin, irregular flakes of C_4AH_{19} hydrate that fills the space between hydrated calcium aluminate crystals.

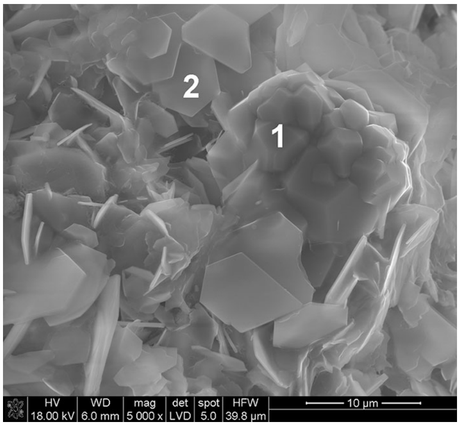

Fig. 11 SEM image of hardened Bi-doped C_7A_3Z cement paste cured at 50 °C for 48 h. EDS analysis in point 1—cubic crystals of C_3AH_6 hydrate and 2—hexagonal crystals of calcium aluminate hydrates

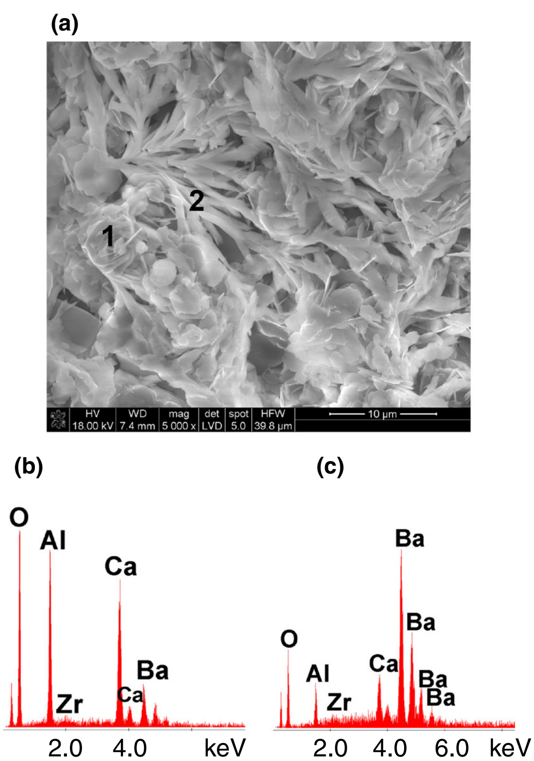

Fig. 12 **a** SEM image of hardened Ba-doped C_7A_3Z cement paste cured at 50 °C for 48 h. EDS analysis in point 1—hexagonal crystals of Ba-doped calcium aluminate hydrates and 2—Ba-rich hydrated aluminate phase. **b** Typical SEM–EDS spectrum of hexagonal crystals of Ba-doped calcium aluminate hydrates in point 1 presented in **a**. **c** Typical SEM–EDS spectrum of crystals of Ba-rich hydrated calcium aluminate phase in point 2 presented in **a**

The EDS analysis of the point 1 (Fig. 12a, b) indicated that the barium was incorporated in Ca–Al hydrates. An additional EDS point analysis made from an elongated crystal indicated that this particle contains mainly Ba, Al and O with minor Ca and can be recognized as Ba-Al hydrates (point 2 in Fig. 12a, c). One valuable conclusion that could be drawn from this experiment is that the metal ions including Ba^{2+}, Cu^{2+} and Bi^{3+} can strongly affect the morphological properties of Ca–Al hydrates.

Conclusions

This research project aimed in the studies of synthesis, reaction mechanism and phases formation during hydration process of novel Ba^{2+}-, Cu^{2+}- or Bi^{3+}-doped $Ca_7ZrAl_6O_{18}$-based fast-setting cements. The complete sintering to melting thermal behavior of the Ba^{2+}-, Cu^{2+}- or Bi^{3+}-doped $Ca_7ZrAl_6O_{18}$ was studied by heating microscopy thermal analysis (HMTA). The hydraulic behaviors and phase evolution were discussed regarding XRD, DSC–TG–EGA–MS and SEM–EDS results. Some general conclusions can be drawn based on the results of this work:

1. Efforts to reduce the sintering temperature of $Ca_7ZrAl_6O_{18}$, resulted in discovery that Cu^{2+} and Bi^{3+} metals additions were effective via liquid phase sintering and activated sintering. The sintering temperature drops to about 1300 °C.
2. Barium doping can increase the thermal resistance of Ba^{2+}-doped $Ca_7ZrAl_6O_{18}$-based cement clinker since the accessory $(Ca,Ba)ZrO_3$ with a perovskite-type structure and $BaAl_2O_4$ phases were also formed.
3. The presence of selected metal ions (Cu^{2+}, Bi^{3+}) created conditions which were favorable for the formation of hexagonal calcium aluminate hydrates rather than the cubic C_3AH_6 one. The role of Ba^{2+} doping ions in this matter was the least noticeable.
4. Microstructural features of cement pastes modified with metal ions including Ba^{2+}, Cu^{2+} and Bi^{3+} were investigated by SEM–EDS. These doping ions strongly affected the morphological properties of Ca–Al hydrates.
5. A group of novel cements containing heavy metals (the metals with their atomic mass heavier than 50) for special applications with new and innovative technologies as components of X-rays and gamma radiation shielding concretes is proposed.

Acknowledgements This project was financed by the National Science Centre, Poland, Project Number 2017/26/D/ST8/00012. The research was performed at Faculty of Materials Science and Ceramics of AGH University of Science and Technology.

References

1. Das SK, Mitra A, Das Poddar PK. Thermal analysis of hydrated calcium aluminates. J Therm Anal Calorim. 1996;47(3):765–74.
2. Rivas Mercury JM, De Aza AH, Pena P. Synthesis of $CaAl_2O_4$ from powders: particle size effect. J Eur Ceram Soc. 2005;25:3269–79.
3. Klaus SR, Neubauer J, Goetz-Neunhoeffer F. How to increase the hydration degree of CA—the influence of CA particle fineness. Cem Concr Res. 2015;67:11–20.
4. Odler I. Special inorganic cements. Boca Raton: CRC Press; 2003.
5. Stephan D, Wistuba S. Crystal structure refinement and hydration behaviour of doped tricalcium aluminate. Cem Concr Res. 2006;36(11):2011–20.
6. Fukuda K, Inoue S, Yoshida H. Cationic substitution in tricalcium aluminate. Cem Concr Res. 2003;33(11):1771–5.
7. Hassaan MY, El-Desoky MM, AbouZeid YM. Estimation of the solubility limit of iron in tricalcium aluminate using different techniques. Mater Sci Eng A. 2000;276(1–2):147–51.
8. Burnett NC, Sharp JH. The hydration of doped tricalcium aluminate. J Mater Sci. 1984;19(6):1980–90.
9. Prodjosantoso AK, Kennedy BJ, Hunter BA. Phase separation induced by hydration of the mixed Ca/Sr aluminates $Ca_{3-x}Sr_xAl_2O_6$: a crystallographic study. Cem Concr Res. 2002;32:647–55.
10. Saikia N, Kato S, Kojima T. Influence of Sn on the hydration of tricalcium aluminate, $Ca_3Al_2O_6$. J Therm Anal Calorim. 2012;109(1):273–86.
11. Ostrowski C, Żelazny J. Solid solutions of calcium aluminates C_3A, $C_{12}A_7$ and CA with sodium oxide. J Therm Anal Calorim. 2004;75(3):867–85.
12. Tian Y, Pan X, Yu H, Tu G. Formation mechanism and crystal simulation of Na_2O-doped calcium aluminate compounds. Trans Nonferr Met Soc China. 2016;26(3):849–58.
13. Prodjosantoso AK, Kennedy BJ. Synthesis and evolution of the crystalline phases in $Ca_{1-x}Sr_xAl_2O_4$. J Solid State Chem. 2002;168:229–36.
14. Pöllmann H, Kaden R. Mono-(strontium-, calcium-) aluminate based cements. In: Fentiman CH, Mangabhai RJ, Scrivener KL, editors. Calcium aluminates proceedings of the international conference. IHS BRE Press; 2014. pp. 99–108.
15. Zhang R, Mao H, Taskinen P. Phase equilibria study and thermodynamic description of the BaO–CaO–Al_2O_3 system. J Am Ceram Soc. 2017;100(6):2722–31.
16. Pöllmann H, Kaden R. X-ray investigations of solid solutions and phase transitions of monocalciumaluminate and monobariumaluminate—use in cement, phosphorescence and radiation protection applications. Adv X-Ray Anal. 2016;59:176–91.
17. Madej D. Synthesis, formation mechanism and hydraulic activity of novel composite cements belonging to the system CaO–Al_2O_3–ZrO_2. J Therm Anal Calorim. 2017;130(3):1913–24.
18. Madej D. Synthesis and hydraulic activity of novel Sr^{2+}-doped $Ca_7ZrAl_6O_{18}$ cement at 50 °C. Thermochim Acta. 2018;661(10):98–105.
19. Madej D. Hydration, carbonation and thermal stability of hydrates in $Ca_{7-x}Sr_xZrAl_6O_{18}$ cement. J Therm Anal Calorim. 2018;131(3):2411–20.
20. Madej D, Szczerba J. Study of the hydration of calcium zirconium aluminate ($Ca_7ZrAl_6O_{18}$) blended with reactive alumina by calorimetry, thermogravimetry and other methods. J Therm Anal Calorim. 2015;121(2):579–88.
21. Madej D, Szczerba J, Nocuń-Wczelik W, Gajerski R, Hodur K. Studies on thermal dehydration of the hydrated $Ca_7ZrAl_6O_{18}$ at different water-solid ratios cured at 60 °C. Thermochim Acta. 2013;569:55–60.
22. Szczerba J, Madej D, Śnieżek E, Prorok R. The application of DTA and TG methods to investigate the non-crystalline hydration products of $CaAl_2O_4$ and $Ca_7ZrAl_6O_{18}$ compounds. Thermochim Acta. 2013;567:40–5.
23. Ukrainczyk N, Matusinovic T, Kurajica S, Zimmermann B, Sipusic J. Dehydration of a layered double hydroxide–C_2AH_8. Thermochim Acta. 2007;464:7–15.
24. Barbakadze VSh, Kozlov VV, Mikul'skii VG, Nikolov II. Durability of building structures and constructions from composite materials. Boca Raton: CRC Press; 1995.
25. Флейшер ГЮ, Токарчук ВВ, Свідерський ВА. The effect of nitrogen-containing organic admixtures on the chemical processes of cement hardening. East Eur J Enterp Technol. 2016;1(6(79)):46–54.
26. Hill RL. The study of hydration of fly ash in the presence of calcium nitrate and calcium formate. Doctoral dissertation. Texas; 1994 (**unpublished research work**).
27. Bushnell-Watson SM, Sharp JH. The detection of the carboaluminate phase in hydrated high alumina cements by differential thermal analysis. Thermochim Acta. 1985;93:613–6.
28. Elving PJ, Winefordner JD, Kolthoff IM. Treatise on analytical chemistry. New York: Wiley; 1993.

Publisher's Note Springer Nature remains neutral with regard to jurisdictional claims in published maps and institutional affiliations.